

Origami Mechanical Metamaterials Based on the Miura-Derivative Fold Patterns

Xiang Zhou^{1*}, Shixi Zang¹, Zhong You²

1 School of Aeronautics and Astronautics, Shanghai Jiao Tong University, No. 800 Dongchuan
Road, Shanghai, 200240, China

2 Department of Engineering Science, University of Oxford, Parks Road, Oxford, OX3 0PL, UK

ABSTRACT

This paper presents two new types of origami-inspired mechanical metamaterials based on the Miura-derivative fold patterns that consist of non-identical parallelogram facets. The analytical models to predict dimension changes and deformation kinematics of the proposed metamaterials are developed. Furthermore, by modelling the creases as revolute hinges with certain rotational spring constants, we derived analytical models for stretching and bulk moduli. The analytical models are validated through FE simulation results. Numerical examples reveal that the proposed metamaterials possess some intriguing properties including negative Poisson's ratios and bulk modulus. The work present in this paper can provide a highly flexible framework for the design of versatile tunable mechanical metamaterials.

Keywords: mechanical metamaterial, Miura-derivative fold pattern, Poisson's ratios, stretching moduli, bulk modulus

* Corresponding author, E-mail: xiangzhou@sjtu.edu.cn, phone: +86-21-34207538, address: School of Aeronautics and Astronautics, No. 800 Dongchuan Road, Shanghai, 200240, China.

1. Introduction

Metamaterials, the man-made materials with unusual physical properties that arise mainly from the arrangement instead of properties of constituent structures, have aroused considerable research interests from scientists and engineers in recent years and open opportunities for many state-of-the-art applications ranging from invisibility cloaks [1-4], to solar photovoltaic system [5,6], seismic protection [7], ultra-effective sound absorption [8,9], and mechanical metamaterials [10-14]. In this context, origami, the art of folding a two-dimensional (2D) sheet into a three-dimensional (3D) structure, offers an inspiring source for designing mechanical metamaterials. Of particular interest here are rigid origami where all facets remain unbent with the creases acting as rotational hinges during continuous folding, and a particular fold pattern, known as the Miura pattern, which is constructed from a single repeated parallelogram facet and is both rigid- and flat-foldable. In the pioneering work, Schenk and Guest [15] reported the deformation kinematics of two folded cellular metamaterials based on the folded Miura pattern, which manifest negative in-plane and positive out-of-plane Poisson's ratios. Wei et al. [16] extended Schenk and Guest's work by considering the rotational stiffness of the creases and derived the stretching and bending rigidities of Miura-folded metamaterials. Later on, Lv et al. [17] showed that the in-plane Poisson's ratio of Miura-folded metamaterials can in fact be both positive and negative when the whole size of the Miura pattern instead of the size of a unit cell is taken into account. Silverberg et al. [18] proposed a reprogrammable single-layered origami metamaterial design by introducing pop-through defects into perfect Miura tessellations. More recently, Li and Wang [19] investigated the pressure-dependent multi-stability properties of an individual fluid-filled tubular cell and its dual cell configuration formed by stacking Miura unit cells. Filipov et al. [20] introduced a new orientation to stack Miura patterns into rigid-foldable zipper-coupled tubes from which reconfigurable cellular metamaterials can be built. In addition to the Miura pattern, Waitukaitis et al. [21] studied the multi-stability characteristics of metasheets consisting of periodic rigid degree-four vertices. Eidini and Paulino [22] proposed a new class of cellular folded metamaterials constructed from the rigid-foldable BCH pattern that combines origami folding with kirigami.

In this paper, we extend the existing work on classic Miura-folded metamaterials to rigid-foldable

Miura-derivative fold patterns [23-25], which comprise quadrilateral facets that are not all identical. We focus here primarily on periodical fold patterns so that the properties of the 3D bulk system can be represented by those of a repeating unit cell, and parallelogram facets because patterns containing non-parallelogram quadrilateral facets will lead to curved or irregular folded shapes [23,24], making it quite challenging if not impossible using them to design mechanical metamaterials. Our work presented herein leads to metamaterial models that not only include conventional Miura-folded metamaterials as the simplest cases but more importantly can be tailored to exhibit a wide range of mechanical properties which would otherwise be difficult to be achieved by existing designs, thus substantially broadening the design space of origami-based mechanical metamaterials.

The layout of this paper is as follows. The geometries of the Miura-derivative unit cell and its stacked unit cell models are first introduced. Based on the stacked unit cell models, two types of Miura-derivative metamaterials are proposed. The analytical models to predict in- and out-of-plane Poisson's ratios, and stretching and bulk moduli of the proposed metamaterials are derived and validated with the finite element (FE) results. The properties of the Miura-derivative metamaterials are discussed through several numerical examples based on a generic piecewise periodic base function. Finally, a brief summary concludes the paper.

2. Unit cell geometry

A typical unit cell of the Miura pattern is illustrated in figure 1a, where the mountain and valley creases are indicated by the blue and red lines or vice versa. It can be defined by the longitudinal and transverse crease lengths a and b and an oblique angle γ_1 . Without loss of generality, γ_1 is always taken as an acute angle throughout the paper. The other oblique angle γ_2 is determined by γ_1 through the relationship $\gamma_1 + \gamma_2 = \pi$ since all the parallelogram facets are identical in this case. If γ_2 and b_2 are made independent of γ_1 and b_1 , a generalized form of the Miura unit cell can be obtained, as shown in figure 1b. Comparable to the Miura pattern, the generalized form has also one degree of freedom of folding motion that can be characterized by a single parameter. Here, we employ $\xi_1 \in [0, \gamma_1]$ (figure 1c) as the parameter to describe folding. The outer dimensions of the folded pattern, defined by the dimensions of the smallest virtual box that can

accommodate the folded pattern, are then given by

$$w = \sum_{i=1}^2 b_i \sqrt{1 - \cos^2 \gamma_i \sec^2 \gamma_1 \cos^2 \xi_1}, \quad (2.1)$$

$$s = \frac{2a \cos \gamma_1}{\cos \xi_1} + v, \quad (2.2)$$

$$h = a \cos \gamma_1 \sqrt{\tan^2 \gamma_1 - \tan^2 \xi_1}, \quad (2.3)$$

where v is determined as

$$v = \max \left\{ b_1 \cos \xi_1, \sum_{i=1}^2 \frac{b_i \cos \gamma_i \cos \xi_1}{\cos \gamma_1} \right\}. \quad (2.4)$$

The detailed derivation of equations (2.1) to (2.4) provided in section A of the electronic supplementary material.

Consider now an arbitrary periodic function $y = f(x)$ with period T , which is referred to as the base function in the sequel. A single period of the base function is first discretized into $N+1$ points A_0, A_1, \dots, A_N , as shown in figure 2a. Re-joining these points with straight-line segments results in a piecewise polyline, upon which a unit cell of a periodic Miura-derivative pattern can be generated, as shown in figure 2b, where the i -th oblique angle γ_i and the i -th transverse crease length b_i are obtained as

$$\gamma_i = \tan^{-1} \left(\frac{\Delta x_i}{f(x_i) - f(x_{i-1})} \right), b_i = \frac{\Delta x_i}{\sin \gamma_i}. \quad (2.5)$$

Again, we employ $\xi_1 \in [0, \gamma_1]$ (figure 2c) to parameterize its folding motion. According to equations (2.1) and (2.2), the outer dimensions w_u and s_u of the folded unit cell are obtained as

$$w_u = \sum_{i=1}^N b_i \sqrt{1 - \cos^2 \gamma_i \sec^2 \gamma_1 \cos^2 \xi_1}, \quad (2.6)$$

$$s_u = \frac{2a \cos \gamma_1}{\cos \xi_1} + v_u, \quad (2.7)$$

where v_u is determined as

$$v_u = \sum_{i=1}^m \frac{b_i \cos \gamma_i \cos \xi_1}{\cos \gamma_1}, \quad (2.8)$$

where $m \in [1, N]$ and $f(x_m) = \max\{f(x_1), \dots, f(x_N)\}$, and the height $h_u = h$.

3. Stacked geometry

Two or more folded Miura-derivative unit cells discussed above of independent heights can be stacked in the z direction, leading to a multi-layered folded structure. There are two types of stacking sequence between successive layers, namely mountain-valley (M-V) stacking and valley-valley (V-V) stacking, as illustrated in figures 3. For both cases, four constraints must be met so that the two layers are practically stackable and the stacked assembly is still rigid-foldable: $b_i^1 = b_i^2$, $i = 1, \dots, N$, $w_u^1 = w_u^2$, $s_u^1 = s_u^2$, and $v_u^1 = v_u^2$, where superscripts 1 and 2 denote the layer numbers. Substituting equations (2.6) to (2.8) into these constraints yields

$$a^1 \cos \gamma_i^1 = a^2 \cos \gamma_i^2, i = 1, \dots, N. \quad (3.1)$$

3D bulk metamaterials can be constructed by repeating the M-V and/or V-V stacked unit cells in all three orthogonal directions. We focus here on two generic models shown in figure 4, each having n_1 stacked unit cells in the in-plane transverse (W) direction, n_2 in the in-plane longitudinal (S) direction and n_3 in the stacking (H) direction. Based on the unit cell geometry discussed above, the total outer dimensions of them can be written as

$$W|_{M-V} = W|_{V-V} = W = n_1 w_u^1, \quad (3.2)$$

$$S|_{M-V} = S|_{V-V} = S = n_2 s_u^1 + (1 - n_2) v_u^1, \quad (3.3)$$

$$H|_{M-V} = n_3 (h_u^2 + h_u^1), \quad (3.4)$$

$$H|_{V-V} = h_u^1 + n_3 (h_u^2 - h_u^1), \quad (3.5)$$

where it is assumed, without loss of generality, that $h_u^2 \geq h_u^1$. The total volume occupied by the bulk system is then obtained as

$$V = W \times S \times H. \quad (3.6)$$

A hand-folded card model of the bulk metamaterials consisting of $3 \times 3 \times 3$ M-V stacked unit cells is shown in the electronic supplementary material movie S1.

4. Poisson's ratios of Miura-derivative metamaterials

The deformation of the Miura-derivative metamaterial can be characterized by an in-plane Poisson's ratio $\nu_{SW} = -\varepsilon_S/\varepsilon_W$ and two out-of-plane Poisson's ratios $\nu_{HW} = -\varepsilon_H/\varepsilon_W$ and $\nu_{HS} = -\varepsilon_H/\varepsilon_S$, where $\varepsilon_W = dW/W$, $\varepsilon_S = dS/S$ and $\varepsilon_H = dH/H$ are the infinitesimal strains in the W , S and H directions, respectively. Using equations (3.2) to (3.5), the Poisson's ratios are obtained as

$$\nu_{SW}|_{M-V} = \nu_{SW}|_{V-V} = - \frac{\left(\frac{2n_2 a^1 \cos \gamma_1^1}{\cos^2 \xi_1} - \sum_{i=1}^m \frac{b_i^1 \cos \gamma_i^1}{\cos \gamma_1^1} \right)}{\left(\sum_{i=1}^N \frac{n_1 b_i^1 \sec \gamma_1^1 \cos^2 \gamma_i^1 \cos \xi_1}{\sqrt{\cos^2 \gamma_1^1 - \cos^2 \gamma_i^1 \cos^2 \xi_1}} \right)} \cdot \frac{W}{S}, \quad (4.1)$$

$$\nu_{HW}|_{M-V} = \frac{n_3 a^1 \left(\frac{1}{\sqrt{\tan^2 \gamma_1^2 - \tan^2 \xi_1}} + \frac{1}{\sqrt{\tan^2 \gamma_1^1 - \tan^2 \xi_1}} \right)}{\left(\sum_{i=1}^N \frac{n_1 b_i^1 \sec^2 \gamma_1^1 \cos^2 \gamma_i^1 \cos^4 \xi_1}{\sqrt{\cos^2 \gamma_1^1 - \cos^2 \gamma_i^1 \cos^2 \xi_1}} \right)} \cdot \frac{W}{H_{M-V}}, \quad (4.2)$$

$$\nu_{HW}|_{V-V} \approx \frac{n_3 a^1 \left(\frac{1}{\sqrt{\tan^2 \gamma_1^2 - \tan^2 \xi_1}} - \frac{1}{\sqrt{\tan^2 \gamma_1^1 - \tan^2 \xi_1}} \right)}{\left(\sum_{i=1}^N \frac{n_1 b_i^1 \sec^2 \gamma_1^1 \cos^2 \gamma_i^1 \cos^4 \xi_1}{\sqrt{\cos^2 \gamma_1^1 - \cos^2 \gamma_i^1 \cos^2 \xi_1}} \right)} \cdot \frac{W}{H_{V-V}}, \quad (4.3)$$

$$\nu_{HS} = -\nu_{HW}/\nu_{SW}, \quad (4.4)$$

where it is assumed in equation (4.3) that $n_3 \gg 1$.

Several immediate findings can be made from equations (4.1) to (4.4). First, for the Poisson's ratios to be real, the square root terms must be positive. As a result, the range for ξ_1 is obtained as

$$\max\{\chi_i\} \leq \xi_1 \leq \min\{\gamma_i^j\}, i = 1, \dots, N, j = 1, 2. \quad (4.5)$$

where χ_i equals zero if $\gamma_i^1 > \gamma_1^1$ or $\cos^{-1}(|\cos \gamma_1^1 / \cos \gamma_i^1|)$ if $\gamma_i^1 \leq \gamma_1^1$. This implies that the Miura-derivative metamaterials are in most cases neither flat-foldable nor developable (i.e. all layers unfold flat at the same time); in other words, their volume will never become zero, a property known as self-locking. Next, ν_{WH} of the M-V stacked metamaterial is always positive, and hence its height will reduce as it expands in the W direction. On the contrary, ν_{WH} of the V-V stacked metamaterial is always negative, making it an auxetic material in the W - H plane.

Third, the in-plane Poisson's ratio may transit from a positive value to negative when

$$\sum_{i=1}^m b_i \cos \gamma_i^1 > 2a^1 \cos^2 \gamma_1^1, n_2 \leq \sum_{i=1}^m \frac{b_i \cos \gamma_i^1}{2a^1 \cos^2 \gamma_1^1}, \quad (4.6)$$

and the critical value for ξ_1 is given by

$$\xi_1 = \cos^{-1} \sqrt{\frac{2n_2 a^1 \cos^2 \gamma_1^1}{\sum_{i=1}^m b_i \cos \gamma_i^1}}. \quad (4.7)$$

If inequality (4.6) is not satisfied, the in-plane Poisson's ratio will always be negative. ν_{HS} may also change signs under the same condition given by inequality (4.6). Therefore, given that n_2 is sufficiently large, all three Poisson's ratios of the V-V stacked metamaterial are negative, implying that it expands in all directions, and for the M-V stacked metamaterial, only the in-plane Poisson's ratio is negative, meaning that the height contracts as the in-plane expansion occurs. Physically, the negative out-of-plane Poisson's ratios found in the V-V stacked metamaterials arise from the coupled stacking order in which the odd-numbered layers having a smaller height are tucked in the even-numbered layers. As the in-plane dimensions of the V-V stacked metamaterials are increased, the separation distance between two adjacent even-numbered layers increases due to flattening of the odd-numbered layers. As a result, the total height of the V-V stacked metamaterial can actually increase, leading to negative out-of-plane Poisson's ratios.

5. Stretching and bulk moduli of Miura-derivative metamaterials

To derive the stretching and bulk moduli of the Miura-derivative metamaterial when it is modelled as rigid origami, we assume that all longitudinal creases in each layer have a hinge spring constant k_1 per unit length, all transverse creases have a hinge spring constant k_2 per unit length, the elastic energy is stored only in the creases which act as rotational hinges, and the total elastic energy U of the metamaterial is the summation of the elastic energy in each layer. As a result, U can be expressed as

$$U = n_3 \sum_{j=1}^2 \left(n_2 \sum_{i=1}^{n_1 N-1} k_1 a^j (\beta_i^j - \beta_{i0}^j)^2 + n_1 (2n_2 - 1) \sum_{i=1}^N \frac{1}{2} k_2 b_i^j (\alpha_i^j - \alpha_{i0}^j)^2 \right), \quad (5.1)$$

where α_i^j and β_i^j are the dihedral angles of the i -th transverse and longitudinal creases in a Miura-derivative unit cell, respectively, α_{i0}^j and β_{i0}^j are the natural dihedral angles in the undeformed state, and the superscript j denotes the layer number in a stacked unit cell. According to the minimum total potential energy principle, the total potential energy E of the metamaterial is then given by

$$E = U - \int_{\xi_{10}}^{\xi_1} f_w \frac{dW}{d\xi_1'} d\xi_1' - \int_{\xi_{10}}^{\xi_1} f_s \frac{dS}{d\xi_1'} d\xi_1' - \int_{\xi_{10}}^{\xi_1} f_h \frac{dH}{d\xi_1'} d\xi_1', \quad (5.2)$$

where f_w , f_s and f_h are the external forces applied in the W , S and H directions, respectively. The external forces at equilibrium state are then obtained using the condition $dE/d\xi_1 = 0$, which reads

$$f_w \frac{dW}{d\xi_1} + f_s \frac{dS}{d\xi_1} + f_h \frac{dH}{d\xi_1} = \frac{dU}{d\xi_1}. \quad (5.3)$$

Using equation (5.3), the uniaxial forces in the W , S and H directions at equilibrium can be determined as

$$\bar{f}_w = \frac{dU}{d\xi_1} \bigg/ \frac{dW}{d\xi_1}, \bar{f}_s = \frac{dU}{d\xi_1} \bigg/ \frac{dS}{d\xi_1}, \bar{f}_h = \frac{dU}{d\xi_1} \bigg/ \frac{dH}{d\xi_1}. \quad (5.4)$$

The stretching moduli of the metamaterial associated with the W , S and H directions are obtained as

$$k_w = \frac{d\sigma_w}{d\varepsilon_w}, k_s = \frac{d\sigma_s}{d\varepsilon_s}, k_h = \frac{d\sigma_h}{d\varepsilon_h}, \quad (5.5)$$

where $\sigma_w = \bar{f}_w/(SH)$, $\sigma_s = \bar{f}_s/(WH)$ and $\sigma_h = \bar{f}_h/(WS)$ are the uniaxial stresses at equilibrium. Finally, the bulk modulus of the metamaterial is obtained as $K_V = -dp/(dV/V)$, where $p = -dU/dV$ is the hydrostatic pressure. The detailed derivations for k_w , k_s , k_h and K_V are provided in section B of the electronic supplementary material.

6. Validation

To validate the analytical models for Poisson's ratios and moduli discussed above, we simulated the motion of a V-V stacked unit cell FE model in ABAQUS[®] (3DS, France), as shown in figure 5. In the FE model, the oblique angles γ^1 and transverse crease lengths b are taken as

$$\gamma^1 \text{ (rad)} = [0.97, 0.65, 0.97, 2.17, 2.49, 2.17], \quad (6.1)$$

$$b \text{ (mm)} = [6.93, 8.49, 6.93, 6.93, 8.49, 6.93]. \quad (6.2)$$

The longitudinal crease lengths a^1 and a^2 and the initial folding angle ξ_{10} are taken as 16 mm, 18 mm and 0.92, respectively. All creases are modelled as revolute hinges with a unified rotational spring constant equal to 0.1 N·mm/rad per mm where two adjacent facets are tied together along their common crease with the rotational degree-of-freedom being set free and the torsional spring is implemented using a revolute-type connector element inserted at the center of the crease. The facets are meshed using S4R shell elements with a thickness and average size of 1 mm and are assigned with a Young's modulus equal to 200 GPa. The nodes on the thick dashed and dash-dotted lines are constrained in the z - and x -directions, respectively and nodes 1 and 2 are

constrained in the y -direction. In the load cases for k_w , k_s and k_h , nodes 2, 3 and 4 are displaced along the x , y and z axis, respectively and the forces acting on them together with the outer dimensions of the model are measured to calculate the Poisson's ratios and moduli using a central difference algorithm. The Poisson's ratios versus W curves and the stiffness curves obtained from the FE simulations and the analytical models are shown in figures 6a and 6b, respectively. An excellent agreement between the FE and analytical results is observed, which provides a solid evidence for the validity of the analytical models.

7. Examples

To demonstrate the properties of Miura-derivative metamaterials, we consider here a piecewise periodic base function shown in figure 7a. A single period of the base function is naturally discretized into $N = 2M$ straight-line segments that have the same projections of length A on the y axis. The acute angles θ_i , $i = 1, 2, \dots, N$, between the straight-line segments and the y axis satisfy the following recursive relationship

$$(\theta_{i+1})^\lambda = \begin{cases} (\theta_i)^\lambda - \delta, & i = 1, 2, \dots, M \\ (\theta_i)^\lambda + \delta, & i = M + 1, \dots, N - 1 \end{cases} \quad (7.1)$$

where $\theta_{max} = \theta_1$, $\theta_{min} = \theta_{M+1}$, $\lambda \neq 0$ and $\delta = \frac{(\theta_{max})^\lambda - (\theta_{min})^\lambda}{M}$. The i -th oblique angle γ_i^1 and transverse crease length b_i of the first layer are obtained as

$$\gamma_i^1 = \begin{cases} \theta_i, & \text{odd } i \\ \pi - \theta_i, & \text{even } i \end{cases} \quad (7.2)$$

$$b_i = A / \cos \theta_i. \quad (7.3)$$

The oblique angles γ_i^2 , $i = 1, 2, \dots, N$, of the second layer are then determined using equation (3.1). A 3D rendering of the bulk metamaterial corresponding to the base function is shown in figure 7b.

It is shown above that the Miura-derivative metamaterials have auxetic material properties, implying that during motion their volume and density will change. Therefore, the capability of the metamaterial to change its volume is of interest. To investigate this property, we employ here $\eta_V = (V_{max} - V_{min}) / V_{max}$ as a measurement. Figure 8a shows η_V versus θ_{min} curves with different θ_{max} values ranging from 30° to 75° where $\lambda = 1$, $A = 5$, $N = 10$, $a_1 = 10$, $a_2 = 15$ and $n_{1,2,3} = 10$. The same values for A , N , a_1 , a_2 and $n_{1,2,3}$ are used throughout

this section. It is shown that the V-V stacked metamaterials have larger volume variations than the M-V stacked metamaterials do. For the V-V stacked cases, the volumetric change increases and decreases with the increases in θ_{min} and θ_{max} , respectively. For the M-V stacked cases, while the volumetric change still increases with the increase in θ_{min} , there exist singular points (the black dots) on the curves, before and after which the minimum volume state switches from $\xi_1 = \xi_{1max}$ to $\xi_1 = \xi_{1min}$ (figure 8b), and the volumetric change increases and then decreases with the increase in θ_{max} . Figure 8c shows η_V versus θ_{min} curves with different λ values where $\theta_{max} = 60^\circ$. For the V-V stacked cases, the volumetric change increases with the decrease in λ . For the M-V stacked cases, it is noted that singular points only exist for positive λ and the volumetric change decreases with the decrease in λ before the singular points and then increases afterwards.

Figure 9 shows the Poisson's ratios versus ξ_1 curves with different θ_{min} values ranging from 45° to 60° where $\theta_{max} = 60^\circ$ and $\lambda = 1$. It is shown that the two out-of-plane Poisson's ratios of the V-V stacked metamaterials are always opposite to those of the M-V stacked counterparts and slightly lower in magnitude than the later. For both of the M-V and V-V stacked cases, the absolute values of the in-plane Poisson's ratio ν_{SW} and the out-of-plane Poisson's ratio ν_{hW} increase with the increase in θ_{min} while θ_{min} has negligible influence on ν_{hs} . The influences of λ on the Poisson's ratios are illustrated in figure 10, where $\theta_{max} = 60^\circ$ and $\theta_{min} = 45^\circ$. It is shown that the ν_{SW} and ν_{hW} versus ξ_1 curves become smoother as λ reduces. Again, λ shows no influence on ν_{hs} .

Of particular interests here are the elastic responses of the Miura-derivative metamaterials. Figure 11 shows the stretching moduli versus ξ_1 curves with different θ_{min} values where $\theta_{max} = 60^\circ$, $\lambda = 1$ and $\xi_{10} = 59.5^\circ$. It is shown that the V-V stacked metamaterials are generally stiffer than the M-V stacked type. As θ_{min} decreases, the in-plane modulus k_s and the through-the-thickness modulus k_h increase while the in-plane modulus k_w initially decreases. For the standard Miura case, i.e. $\theta_{min} = \theta_{max}$, k_w reduces to zero as ξ_1 decreases whereas for other cases, k_w becomes infinite at both lower and upper bounds of ξ_1 . Figure 12 shows the influences of λ on the stretching moduli where $\theta_{max} = 60^\circ$, $\theta_{min} = 45^\circ$ and $\xi_{10} = 59.5^\circ$. It is

shown that k_w increases and k_s and k_h decrease with the increase in λ . Finally, the influences of θ_{min} and λ on the bulk modulus K_v are illustrated in figures 13a and b, respectively. It is shown that K_v increases as θ_{min} decreases while it first increases and then decreases as λ decreases. It is interesting to note that the bulk moduli of the V-V stacked metamaterials are always positive while those of the M-V stacked metamaterials range from negative infinity to positive infinity. This unusual property of the M-V stacked metamaterials arises from the fact that the volume V in this case is not a monotonic function of ξ_1 (see figure 8b). Setting $dV/d\xi_1 = 0$ allows us to determine the critical value of ξ_1 at which the bulk modulus of the M-V stacked metamaterial shifts from $+\infty$ to $-\infty$.

8. Summary and final remark

In this paper, we have used the patterns consisting of non-identical parallelogram facets to design 3D mechanical metamaterials. Depending on the stacking sequence between successive layers, two types of metamaterials are proposed. We show that the dimension changes of the proposed metamaterials can be parameterized by a single folding parameter ξ_1 , based on which the analytical models to predict deformation kinematics characterized by Poisson's ratios are developed. Moreover, introducing rotational spring constants to the creases that are modelled as revolute hinges enables us to obtain analytical expressions for stretching and bulk moduli of the proposed metamaterials.

The intriguing properties of the Miura-derivative metamaterials are demonstrated through several numerical examples based on a periodic piecewise base function. The main findings include: a) the Miura-derivative metamaterials possess the self-locking property arising from the restraints on the folding parameter ξ_1 ; b) the V-V stacked metamaterials are subjected to greater volume variations and have higher stretching stiffness than the M-V stacked ones; c) the V-V stacked metamaterials have negative Poisson's ratios in all three orthogonal planes whereas only the in-plane Poisson's ratio of the M-V stacked ones is negative; d) the Miura-derivative metamaterials have infinite stretching and bulk moduli wherein the bulk modulus of the M-V stacked metamaterials even varies from $-\infty$ to $+\infty$, which may lead to some unique vibration and acoustic behaviors [26]. In generally, the geometric and mechanical properties of the

Miura-derivative metamaterials have a broad design space, varying among different sets of base function parameters and folding states, not to mention that there are numerous other possible base function forms that have not been investigated. In this context, our work provides a highly flexible framework for the design of versatile tunable mechanical metamaterials. Moreover, by taking the limit of Δx_i in figure 2a towards zero, the piecewise polyline in figure 2b will eventually convert into a smooth curve of arbitrary shape and the folding of the longitudinal creases into the bending of an infinite narrow strip of the sheet material along each crease. In this manner, the work presented in this paper opens opportunity for the future study of curved-creased metamaterials.

Data accessibility

The electronic supplementary material is available via <http://rspa.royalsocietypublishing.org>.

Competing interests

We have no competing interests.

Authors' contributions

X.Z. designed the study, carried out the analysis and drafted the manuscript; S.Z. derived the equations and made the physical model; Z.Y. conceived of the study and commented on the manuscript. All authors gave final approval for publication.

Acknowledgement

X.Z. wishes to acknowledge the financial support from National Science Foundation of China (No. 51408357).

Funding

X.Z. is funded by National Science Foundation of China (No. 51408357).

References

- [1] Schurig, D., Mock, J. J., Justice, B. J., Cummer, S. A., Pendry, J. B., Starr, A. F. & Smith, D. R. 2006 Metamaterial electromagnetic cloak at microwave frequencies. *Science* **314**, 977-980. (doi:

10.1126/science.1133628)

[2] Soukoulis, C. M., Linden, S. & Wegener, M. 2007 Negative refractive index at optical wavelengths. *Science* **315**, 47-49. (doi: 10.1126/science.1136481)

[3] Cai, W., Chettiar, U. K., Kildishev, A. V. & Shalaev, V. M. 2007 Optical cloaking with metamaterials. *Nat. Photonics* **1**, 224-227. (doi: 10.1038/nphoton.2007.28)

[4] Soukoulis, C. M. & Wegener, M. 2011 Past achievements and future challenges in the development of three-dimensional photonic metamaterials. *Nat. Photonics* **5**, 523-530. (doi: 10.1038/nphoton.2011.154)

[5] Vora, A., Gwamuri, J., Pala, N., Kulkarni, A., Pearce, J. M. & Güney, D. Ö. 2014 Exchanging Ohmic Losses in Metamaterial Absorbers with Useful Optical Absorption for Photovoltaics. *Sci. Rep.* **4**, 4901. (doi: 10.1038/srep04901)

[6] Wu, C., Neuner III, B., John, J., Milder, A., Zollars, B., Savoy, S. & Shvets, G. 2012 Metamaterial-based integrated plasmonic absorber/emitter for solar thermo-photovoltaic systems. *J. Optics* **14**, 024005. (doi: 10.1088/2040-8978/14/2/024005)

[7] Brûlé, S., Javelaud, E. H., Enoch, S. & Guenneau, S. 2014 Experiments on seismic metamaterials: molding surface waves. *Phys. Rev. Lett.* **112**, 133901. (doi: 10.1103/PhysRevLett.112.133901)

[8] Chen, H. & Chan, C. T. 2007 Acoustic cloaking in three dimensions using acoustic metamaterials. *Appl. Phys. Lett.* **91**, 183518. (doi: 10.1063/1.2803315)

[9] Mei, J., Ma, G., Yang, M., Yang, Z., Wen, W. & Sheng, P. 2012 Dark acoustic metamaterials as super absorbers for low-frequency sound. *Nat. Commun.* **3**, 756. (doi: 10.1038/ncomms1758)

- [10] Lee, J. B., Peng, S., Yang, D., Roh, Y. H., Funabashi, H., Park, N., Rice, E. J., Chen, L., Long, R., Wu, M. & Luo, D. 2012 A mechanical metamaterial made from a DNA hydrogel. *Nat. Nanotechnol.* **7**, 816-820. (doi: 10.1038/NNANO.2012.211)
- [11] Bertoldi, K., Reis, P. M., Willshaw, S. & Mullin, T. 2010 Negative poisson's ratio behavior induced by an elastic instability. *Adv. Mater.* **22**, 361-366. (doi: 10.1002/adma.200901956)
- [12] Kadic, M., Bückmann, T., Stenger, N., Thiel, M. & Wegener M. 2012 On the practicability of pentamode mechanical metamaterials. *Appl. Phys. Lett.* **100**, 191901. (doi: 10.1063/1.4709436)
- [13] Lee, J. H., Singer, J. P. & Thomas, E. L. 2012 Micro-/nanostructured mechanical metamaterials. *Adv. Mater.* **24**, 4782-4810. (doi: 10.1002/adma.201201644)
- [14] Zheng, X., Lee, H., Weisgraber, T. H., Shusteff, M., Deotte, J., Duoss, E. B., Kuntz, J. D., Biener, M. M., Ge, Q., Jackson, J. A., Kucheyev, S. O., Fang, N. X. & Spadaccini, C. M. 2014 Ultralight, ultrastiff mechanical metamaterials. *Science* **344**, 1373-1377. (doi: 10.1126/science.1252291)
- [15] Schenk, M. & Guest, S. D. 2013 Geometry of Miura-folded metamaterials. *P. Natl. Acad. Sci. USA.* **110**, 3276-3281. (doi: 10.1073/pnas.1217998110)
- [16] Wei, Z. Y., Guo, Z. V., Dudte, L., Liang, H. Y. & Mahadevan, L. 2013 Geometric mechanics of periodic pleated origami. *Phys. Rev. Lett.* **110**, 215501. (doi: 10.1103/PhysRevLett.110.215501)
- [17] Ly, C., Krishnaraju, D., Konjevod, G., Yu, H. & Jiang, H. 2014 Origami based mechanical metamaterials. *Sci. Rep.* **4**. (doi: 10.1038/srep05979)
- [18] Silverberg, J. L., Evans, A. A., McLeod, L., Hayward, R. C., Hull, T., Santangelo, C. D. & Cohen, I. 2014 Using origami design principles to fold reprogrammable mechanical metamaterials. *Science* **345**, 647-650. (doi: 10.1126/science.1252876)

- [19] Li, S. & Wang, K. W. 2015 Fluidic origami with embedded pressure dependent multi-stability: a plant inspired innovation. *J. R. Soc. Interface* **12**, 20150639. (doi: 10.1098/rsif.2015.0639)
- [20] Filipov, E. T., Tachi, T. & Paulino, G. H. 2015 Origami tubes assembled into stiff, yet reconfigurable structures and metamaterials. *P. Natl. Acad. Sci. USA*. **112**(40), 12321-12326. (doi: 10.1073/pnas.1509465112)
- [21] Waitukaitis, S., Menaut, R., Chen, B. G. G., & van Hecke, M. 2015 Origami multistability: From single vertices to metasheets. *Phys. Rev. Lett.* **114**, 055503. (doi: 10.1103/PhysRevLett.114.055503)
- [22] Eidini, M., & Paulino, G. H. 2015 Unraveling metamaterial properties in zigzag-base folded sheets. *Sci. Adv.* **1**(8), e1500224. (doi: 10.1126/sciadv.1500224)
- [23] Tachi, T. 2009 Generalization of rigid foldable quadrilateral mesh origami. In *Proceedings of the International Association for Shell and Spatial Structures (IASS) Symposium, Valencia, Spain, 28 September-2 October*, pp. 2287-2294.
- [24] Gattas, J. M., Wu, W. & You, Z. 2013 Miura-base rigid origami: parameterizations of first-level derivative and piecewise geometries. *J. Mech. Des.* **135**, 111011. (doi: 10.1115/1.4025380)
- [25] Gattas, J. M. & You, Z. 2014 Miura-base rigid origami: parametrizations of curved-crease geometries. *J. Mech. Des.* **136**, 121404. (doi: 10.1115/1.4028532)
- [26] Liu, X. N., Hu, G. K., Huang, G. L. & Sun, C. T. 2011 An elastic metamaterial with simultaneously negative mass density and bulk modulus. *Appl. Phys. Lett.* **98**, 251907. (doi: 10.1063/1.3597651)

List of figures

- Figure 1 (a) A typical unit cell of the Miura pattern; (b) A generalized Miura unit cell pattern; (c) The folded state of a generalized Miura unit cell.
- Figure 2 (a) A single period of a periodic base function $y = f(x)$ with period T ; (b) A unit cell of a periodic Miura-derivative pattern; (c) The folded state of a Miura-derivative unit cell.
- Figure 3 (a) A M-V stacked unit cell; (b) A V-V stacked unit cell.
- Figure 4 (a) M-V and (b) V-V stacked metamaterials consisting of n_1 stacked unit cells in the in-plane transverse (W) direction, n_2 in the in-plane longitudinal (S) direction and n_3 in the stacking (H) direction.
- Figure 5 A V-V stacked unit cell finite element model.
- Figure 6 (a) The Poisson's ratios versus W curves and (b) the stiffness versus W curves obtained from the FE simulations and the analytical models.
- Figure 7 (a) A piecewise periodic base function defined by equation (7.1); (b) A 3D rendering of the bulk metamaterial corresponding to the base function.
- Figure 8 (a) η_V versus θ_{min} curves with different θ_{max} values where $\lambda = 1$, $A = 5$, $N = 10$, $a_1 = 10$, $a_2 = 15$ and $n_{1,2,3} = 10$; (b) V/V_{max} versus ξ_1 curves at P_1 , P_2 and P_S ; (c) η_V versus θ_{min} curves with different λ values where $\theta_{max} = 60^\circ$, $A = 5$, $N = 10$, $a_1 = 10$, $a_2 = 15$ and $n_{1,2,3} = 10$.
- Figure 9 (a) ν_{SW} , (b) ν_{hW} and (c) ν_{hs} versus ξ_1 curves with different θ_{min} values where $\theta_{max} = 60^\circ$, $\lambda = 1$, $A = 5$, $N = 10$, $a_1 = 10$, $a_2 = 15$ and $n_{1,2,3} = 10$.
- Figure 10 (a) ν_{SW} , (b) ν_{hW} and (c) ν_{hs} versus ξ_1 curves with different λ values where $\theta_{max} = 60^\circ$, $\theta_{min} = 45^\circ$, $A = 5$, $N = 10$, $a_1 = 10$, $a_2 = 15$ and $n_{1,2,3} = 10$.
- Figure 11 (a) k_W , (b) k_S and (c) k_h versus ξ_1 curves with different θ_{min} values where $\theta_{max} = 60^\circ$, $\lambda = 1$, $\xi_{10} = 59.5^\circ$, $A = 5$, $N = 10$, $a_1 = 10$, $a_2 = 15$ and $n_{1,2,3} = 10$.
- Figure 12 (a) k_W , (b) k_S and (c) k_h versus ξ_1 curves with different λ values where $\theta_{max} = 60^\circ$, $\theta_{min} = 45^\circ$, $\xi_{10} = 59.5^\circ$, $A = 5$, $N = 10$, $a_1 = 10$, $a_2 = 15$ and $n_{1,2,3} = 10$.

$$n_{1,2,3} = 10.$$

Figure 13 (a) K_V versus ξ_1 curves with different θ_{min} values where $\theta_{max} = 60^\circ$, $\lambda = 1$, $\xi_{10} = 59.5^\circ$, $A = 5$, $N = 10$, $a_1 = 10$, $a_2 = 15$ and $n_{1,2,3} = 10$; (b) K_V versus ξ_1 curves with different λ values where $\theta_{max} = 60^\circ$, $\theta_{min} = 45^\circ$, $\xi_{10} = 59.5^\circ$, $A = 5$, $N = 10$, $a_1 = 10$, $a_2 = 15$ and $n_{1,2,3} = 10$.

Figure 1

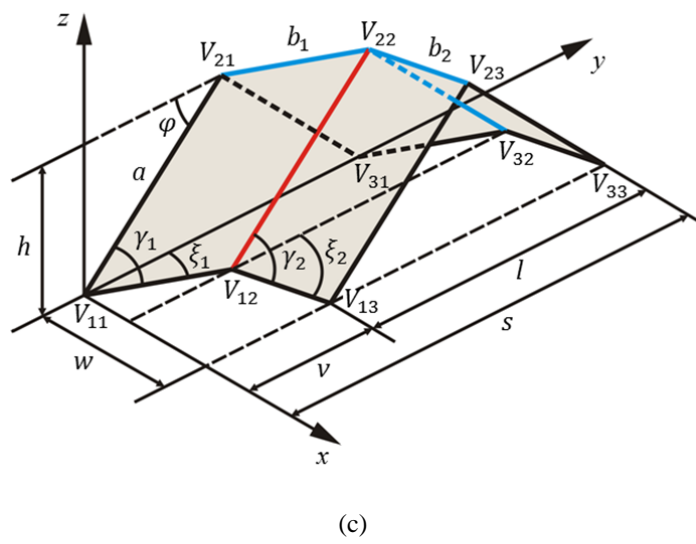
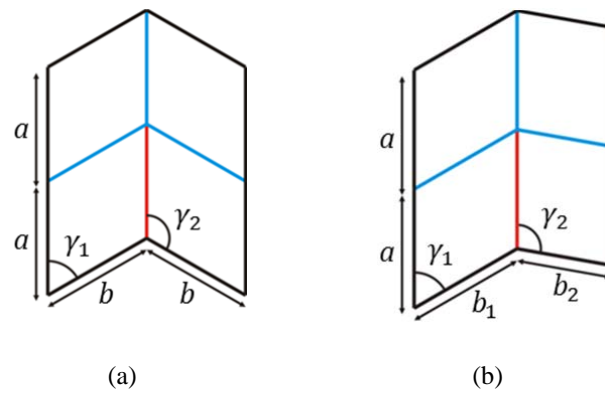


Figure 2

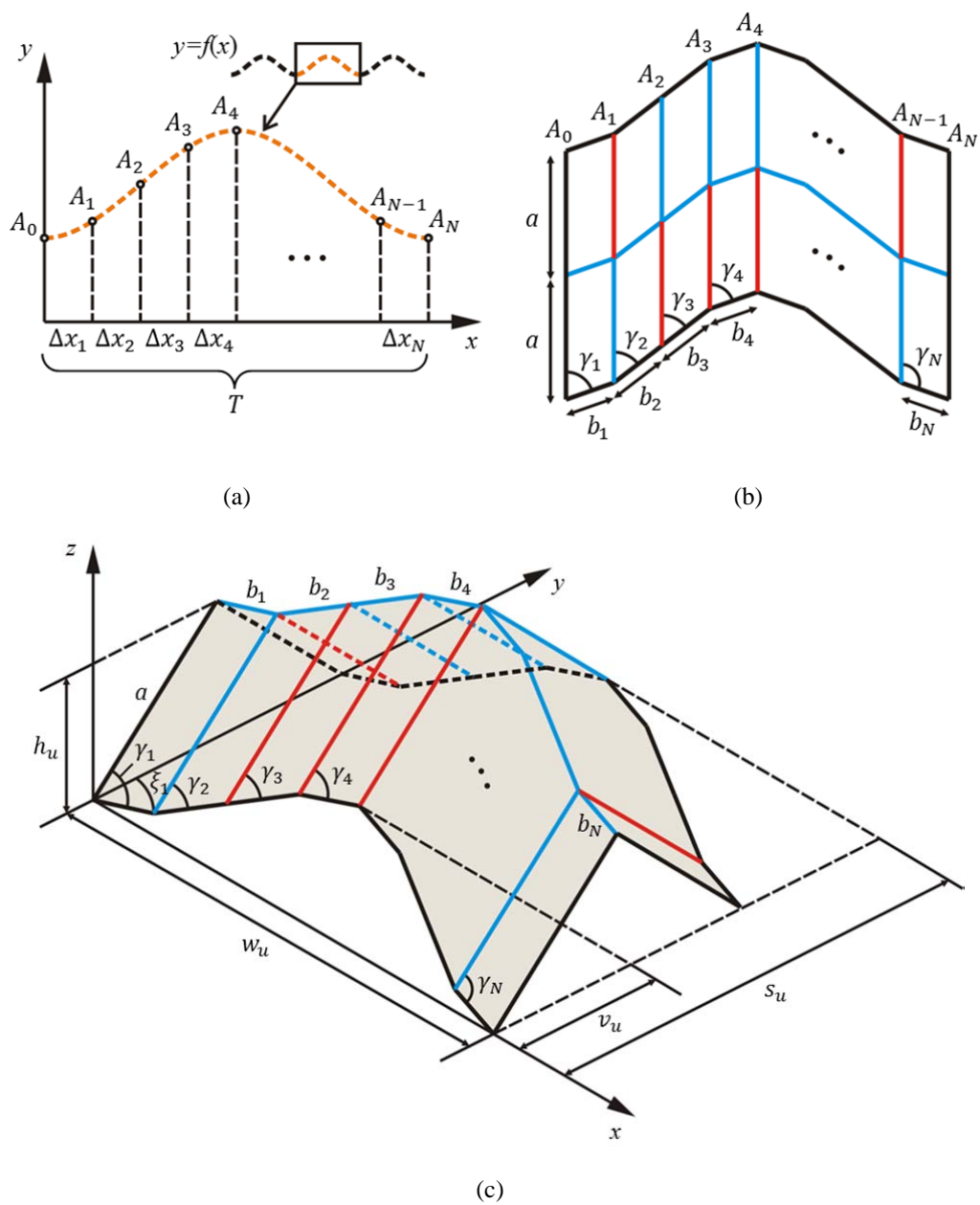


Figure 3

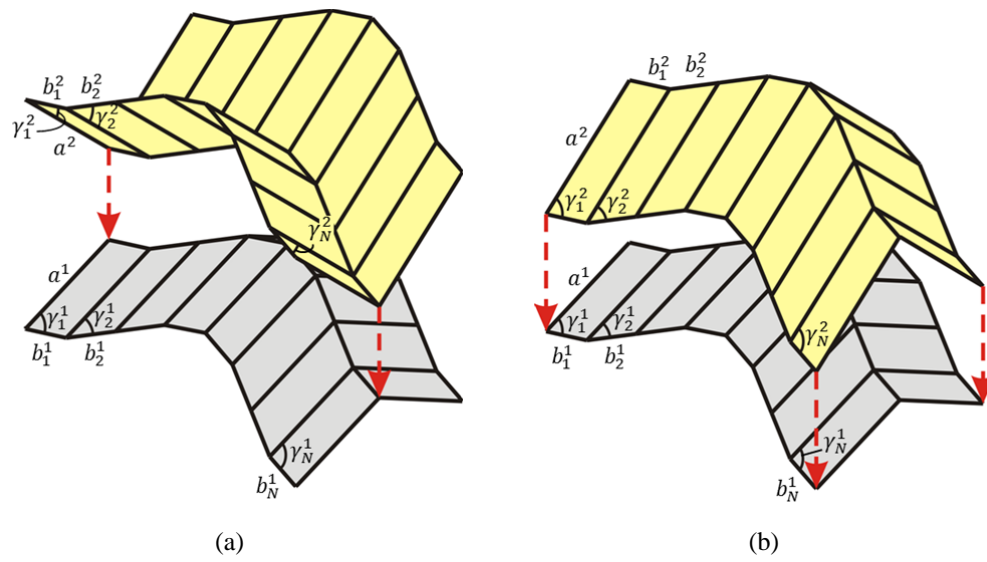


Figure 4

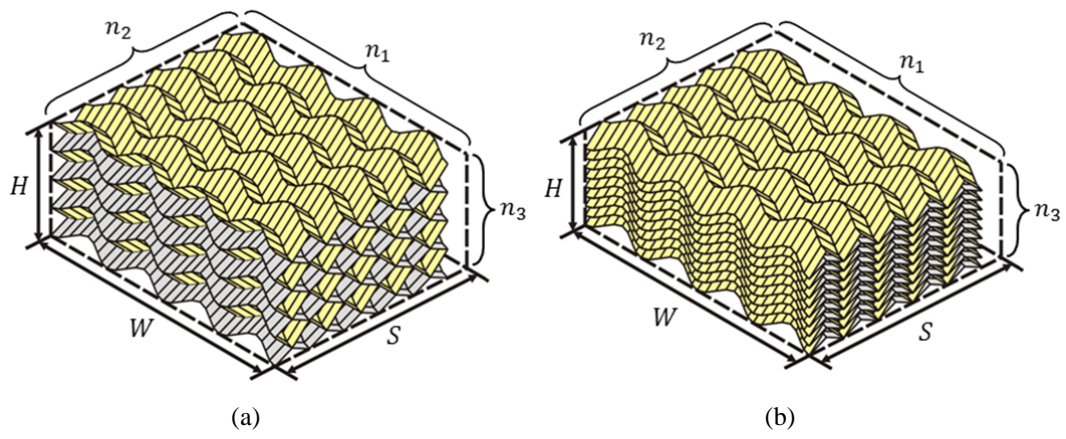


Figure 5

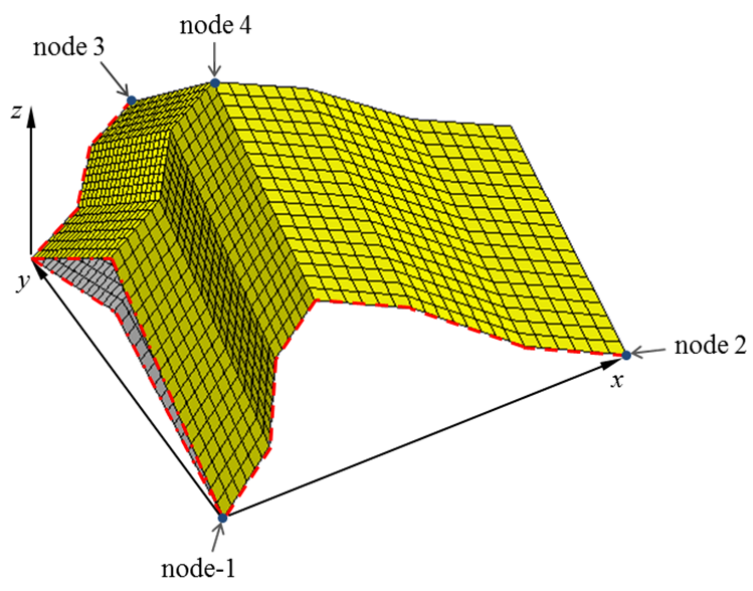
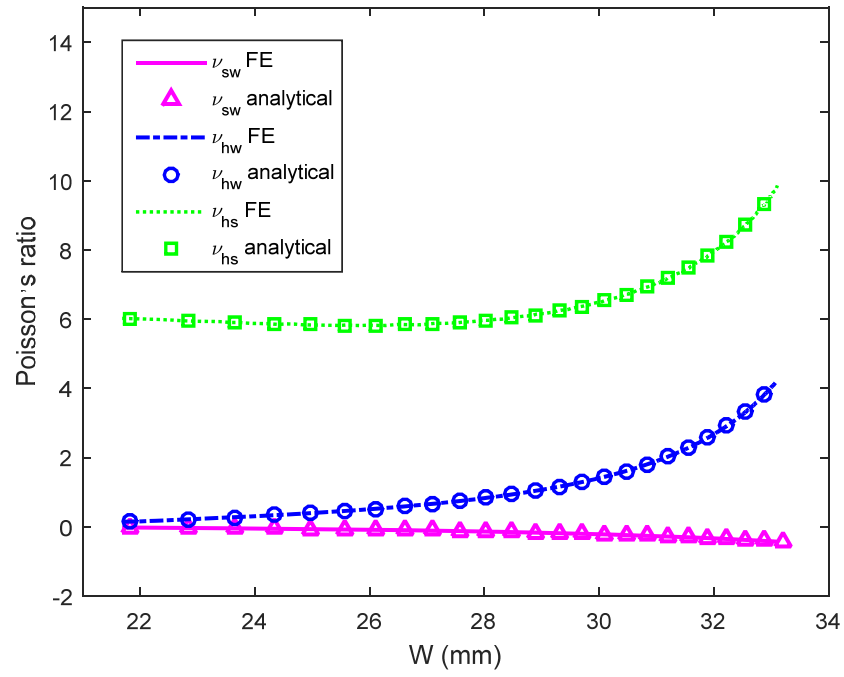
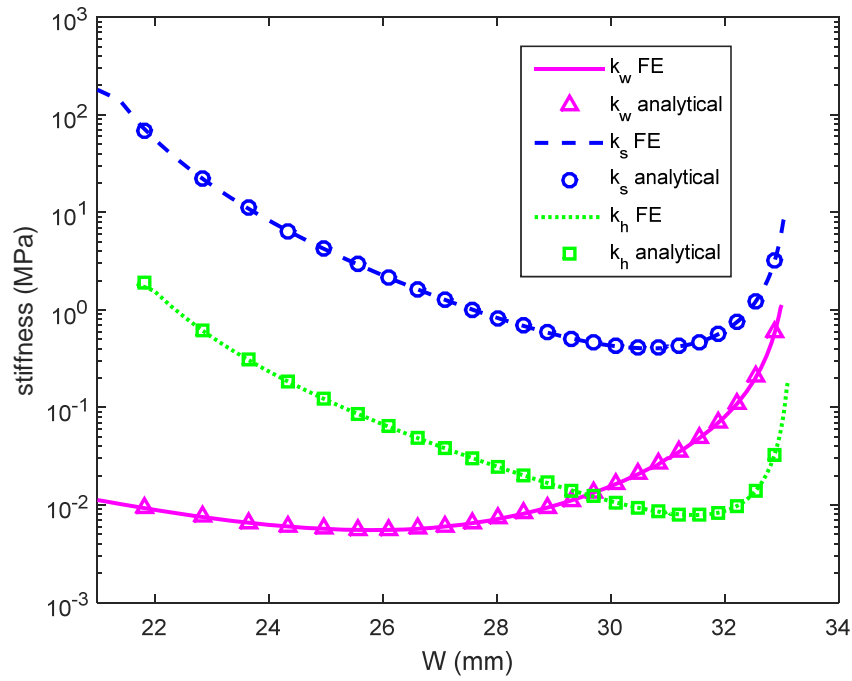


Figure 6

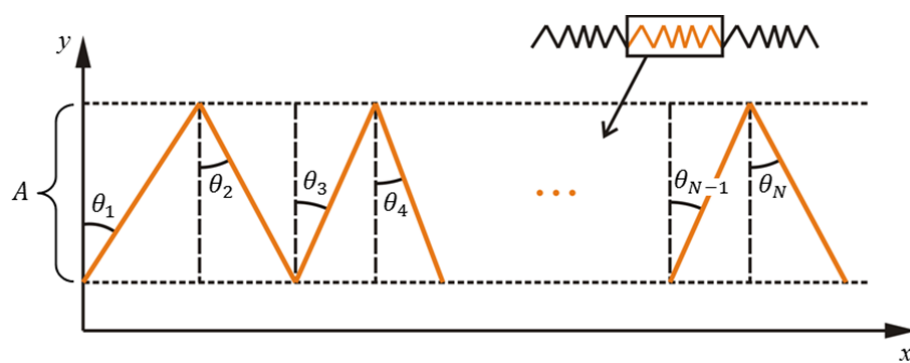


(a)

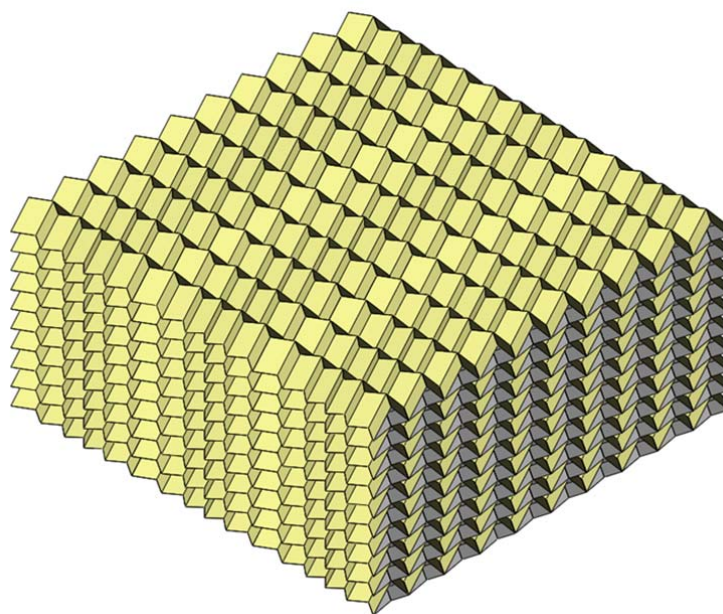


(b)

Figure 7

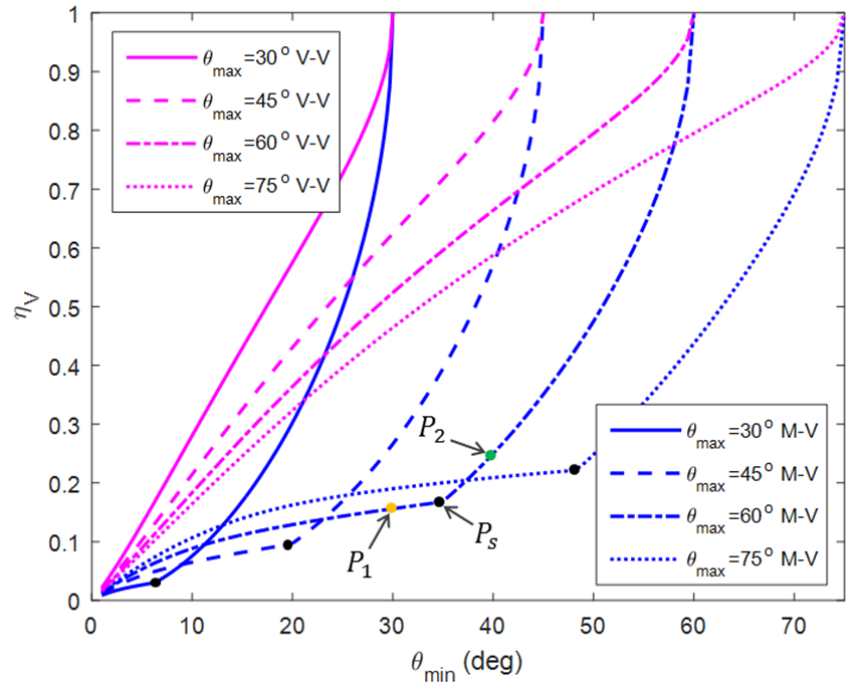


(a)

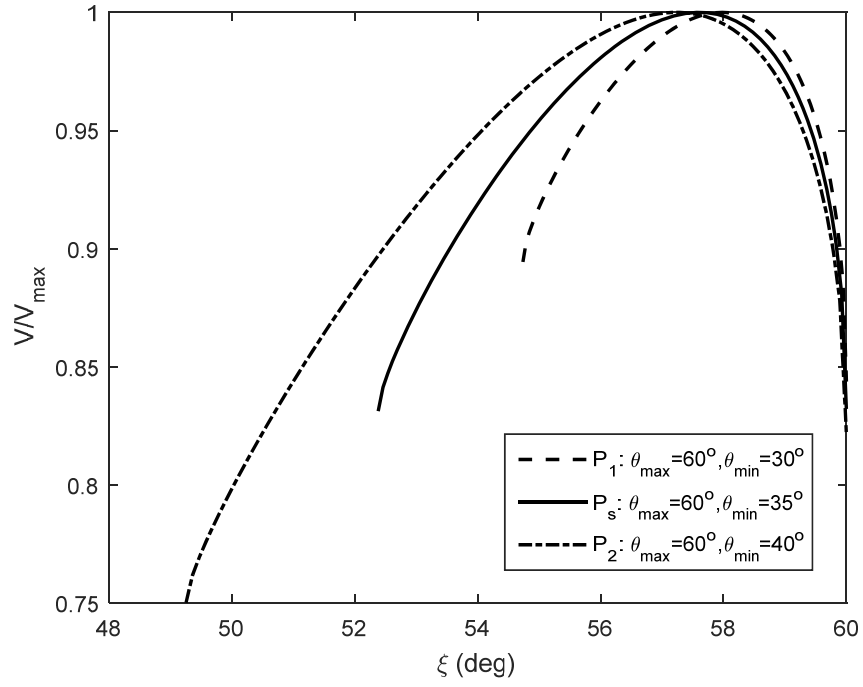


(b)

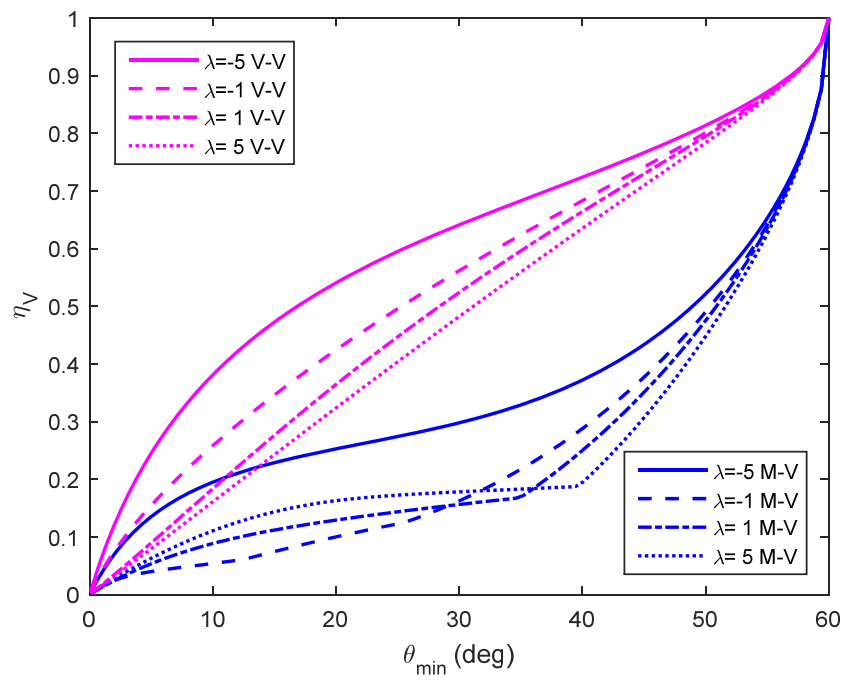
Figure 8



(a)

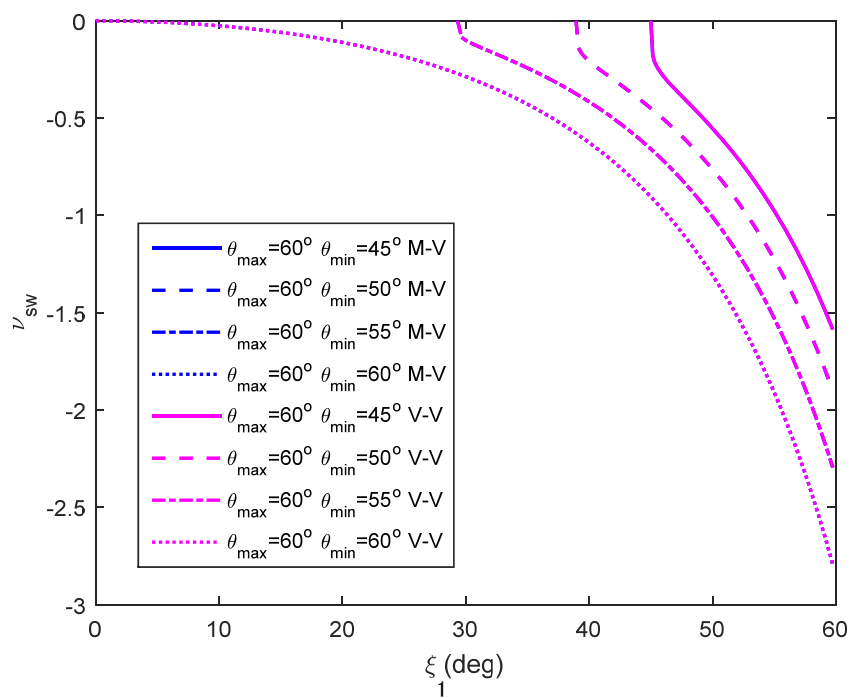


(b)¹

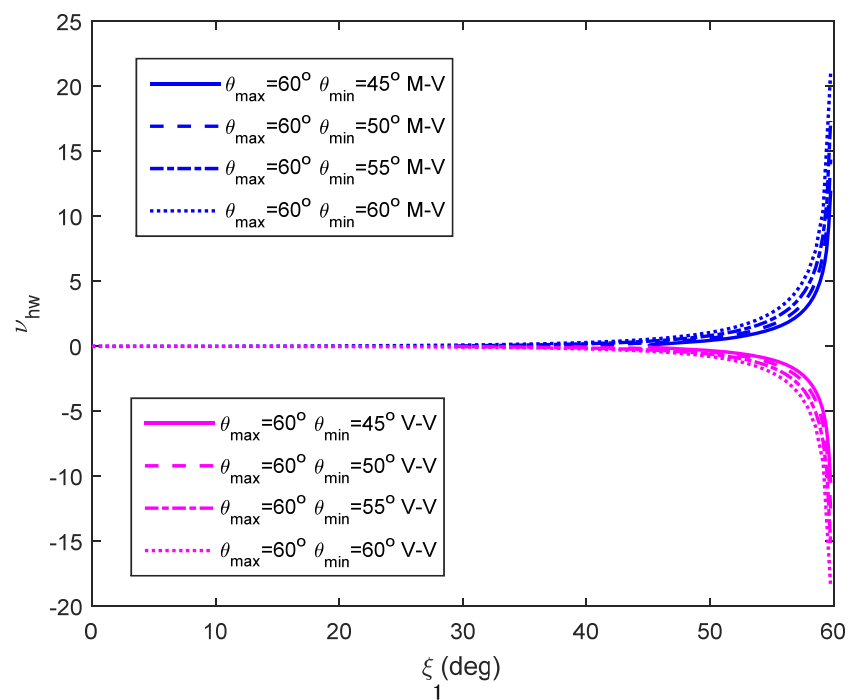


(c)

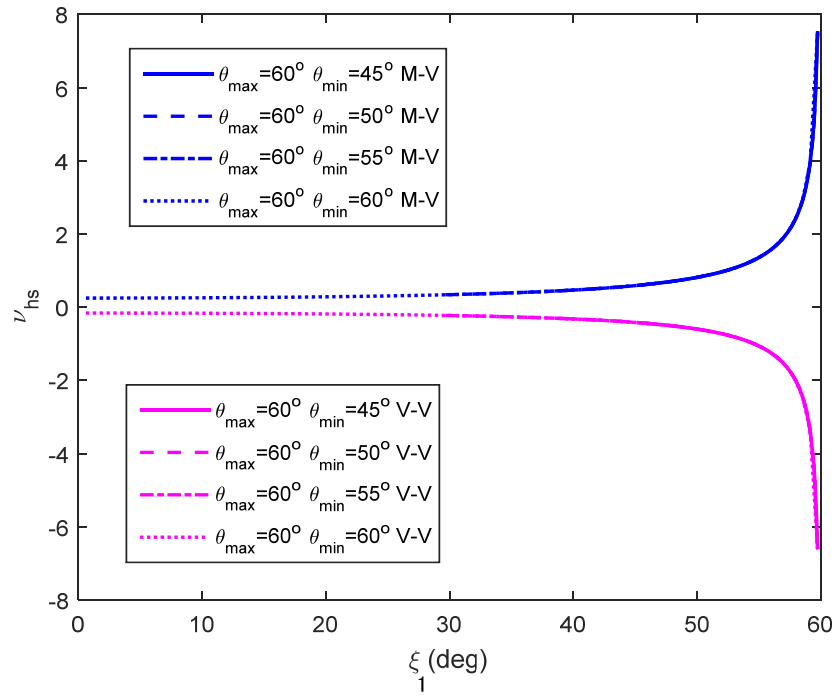
Figure 9



(a)

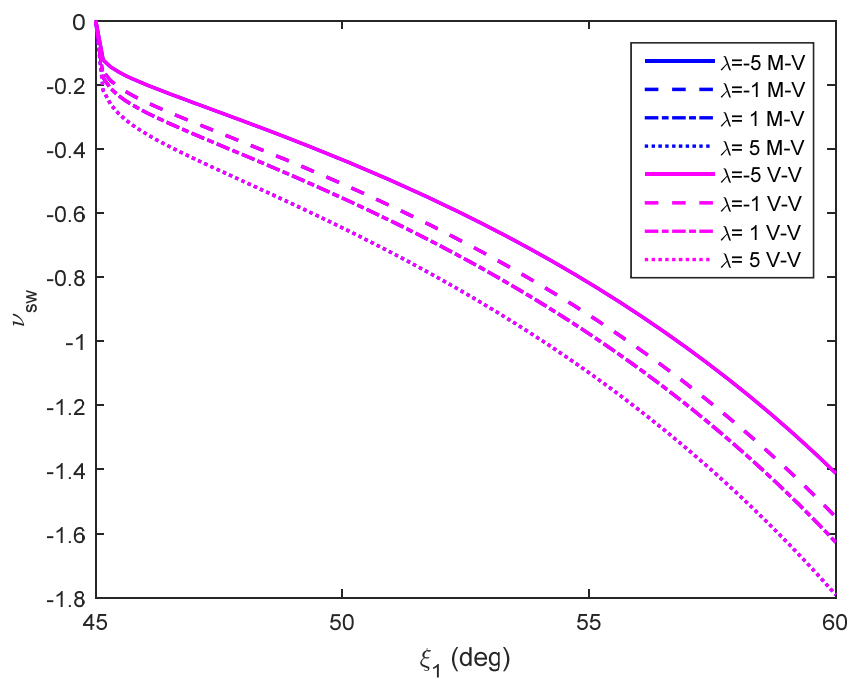


(b)

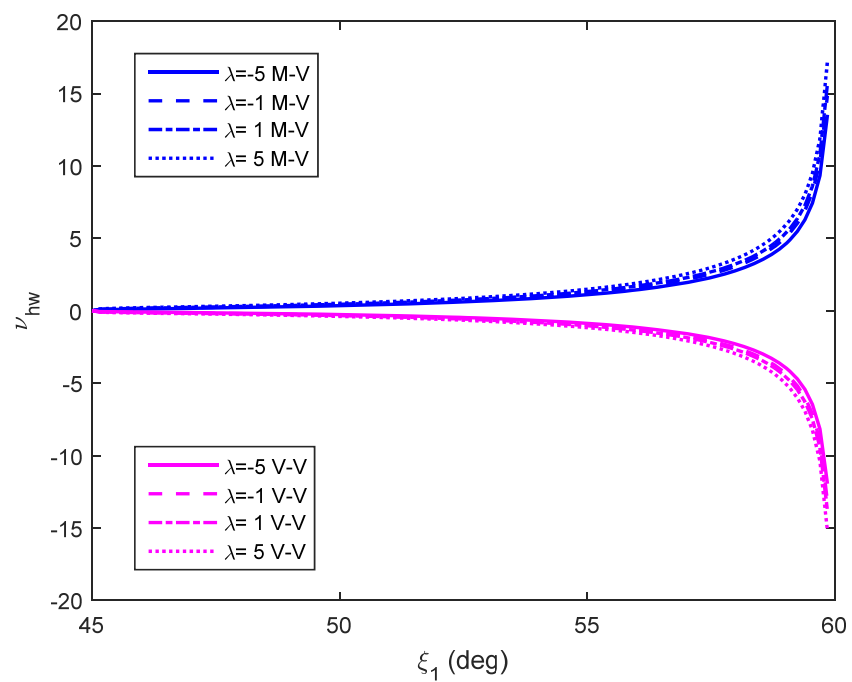


(c)

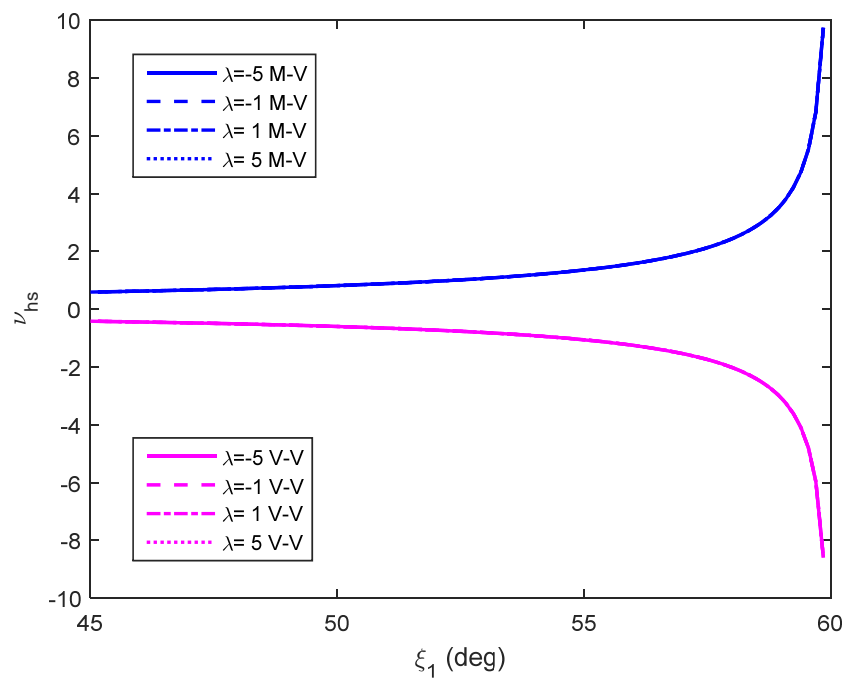
Figure 10



(a)

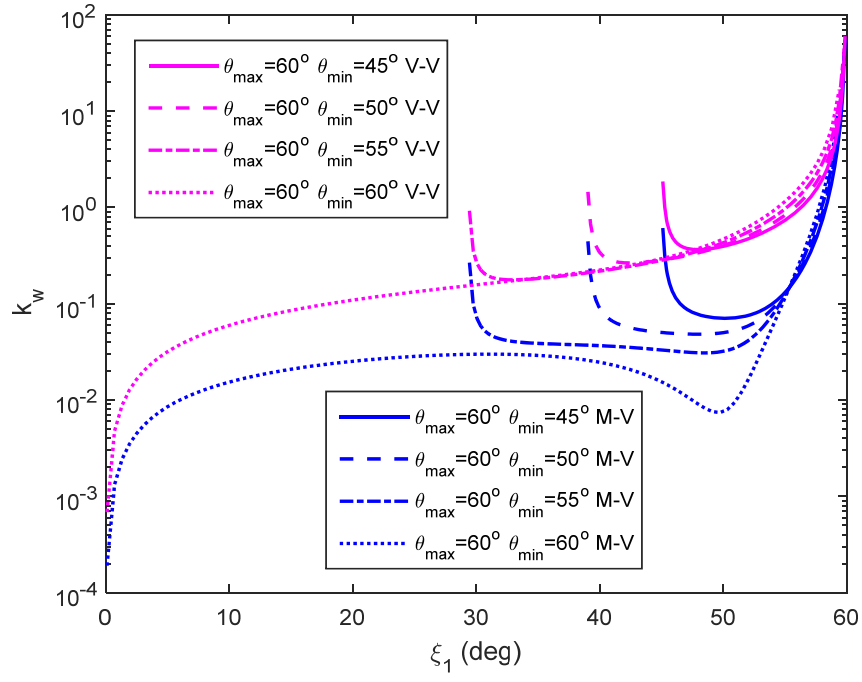


(b)

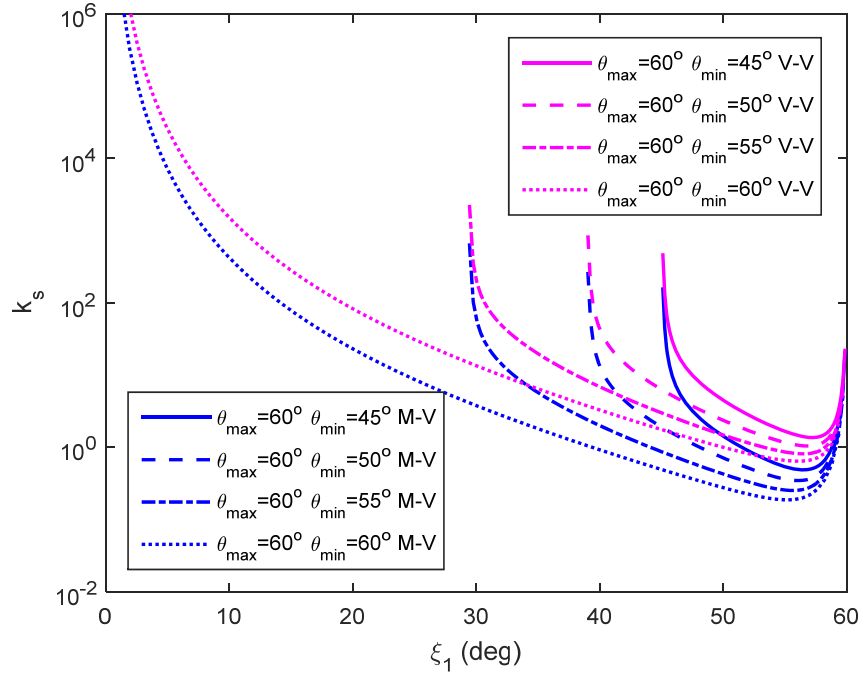


(c)

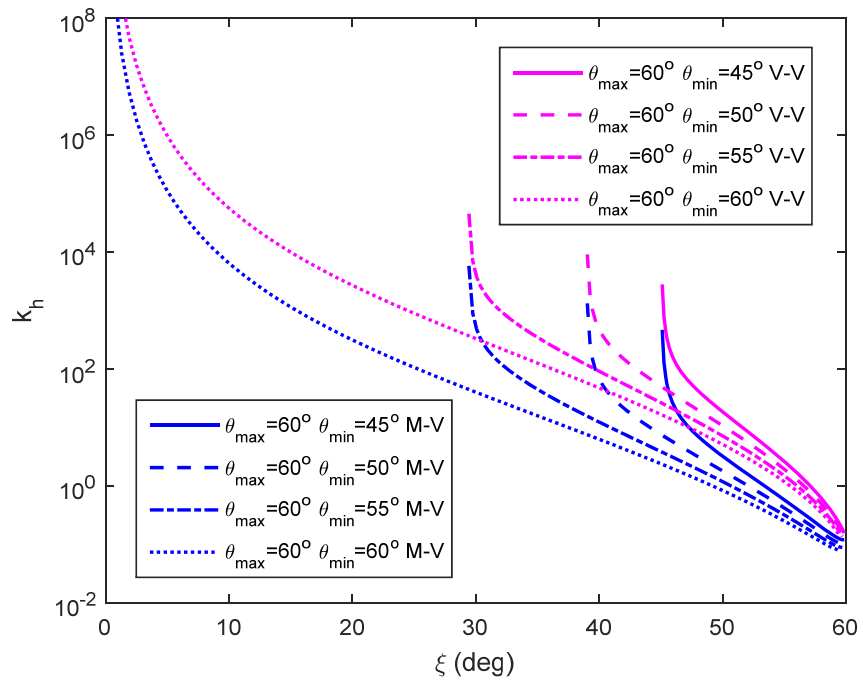
Figure 11



(a)

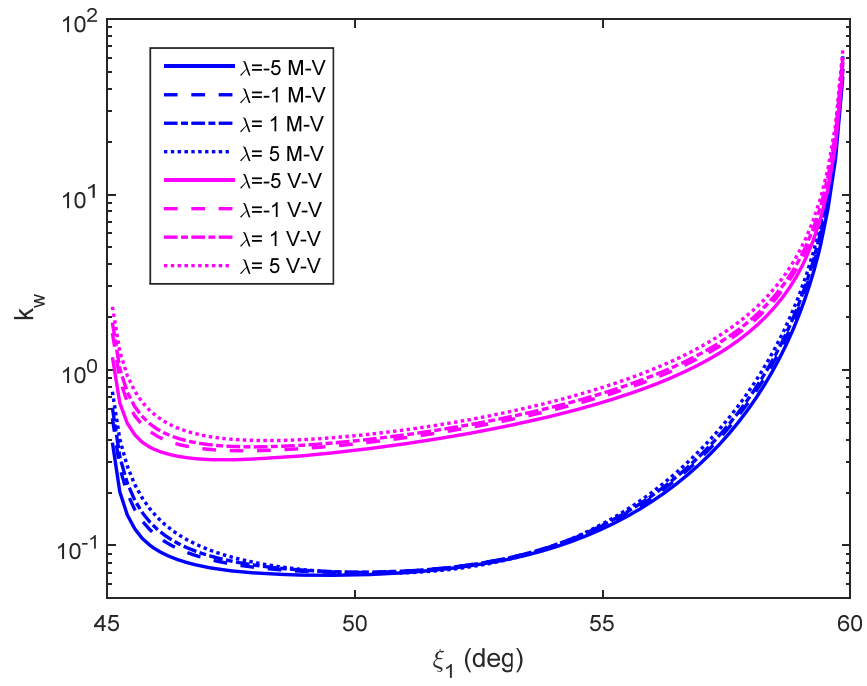


(b)

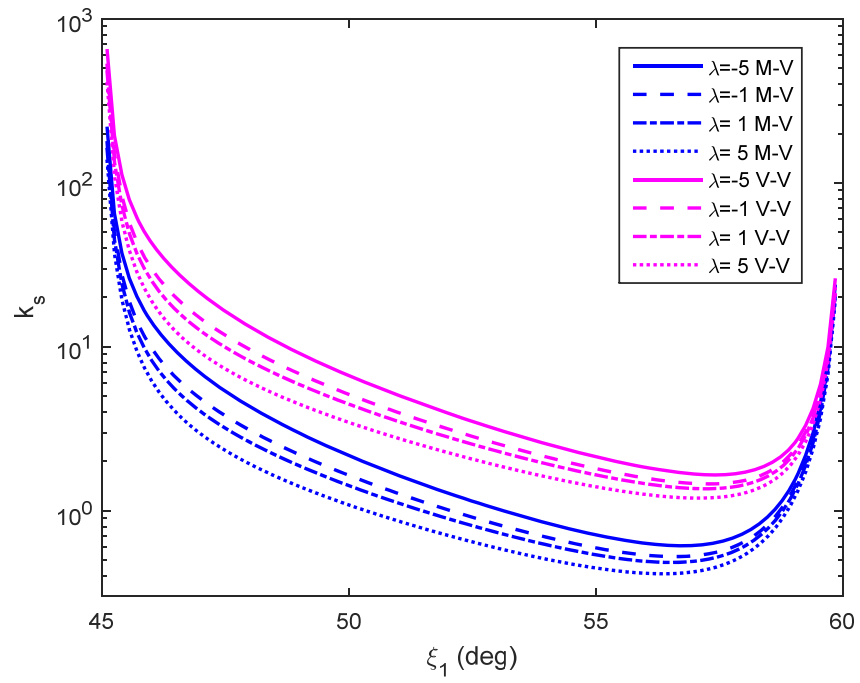


(c)

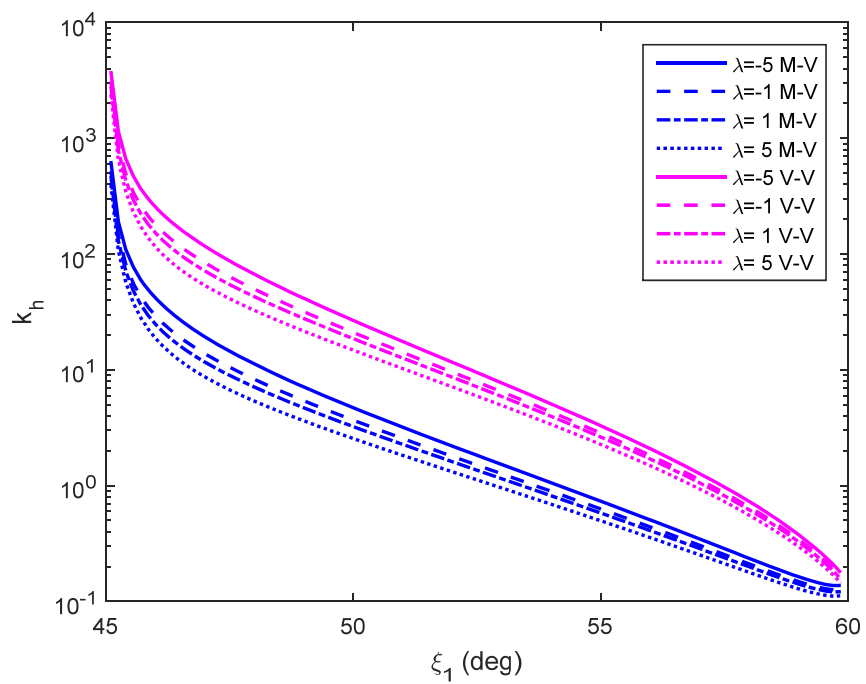
Figure 12



(a)

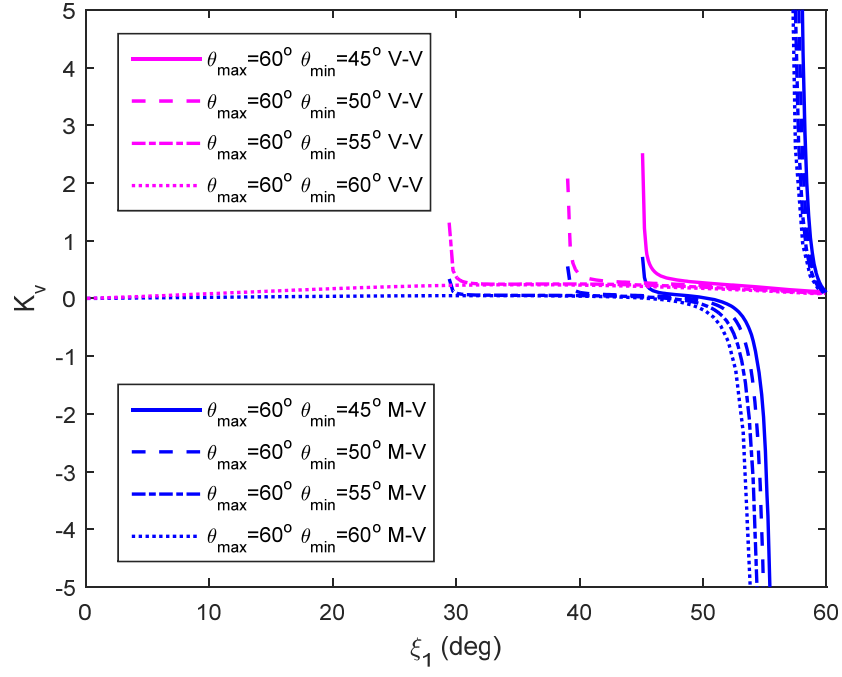


(b)

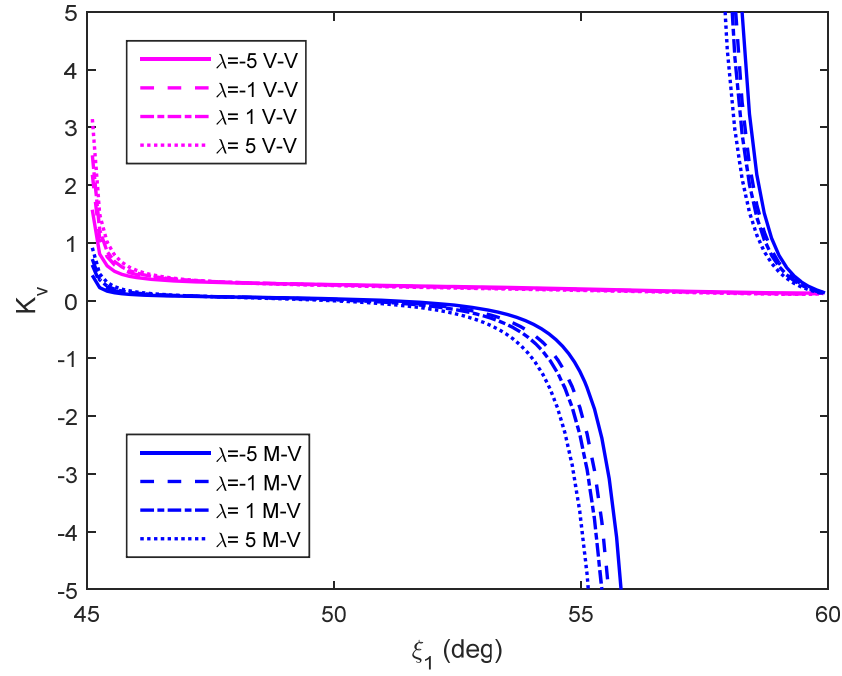


(c)

Figure 13



(a)



(b)

SUPPLEMENTARY MATERIAL FOR

Origami Mechanical Metamaterials Based on the Miura-Derivative Fold Patterns

Xiang Zhou^{1*}, Shixi Zang¹, Zhong You²

1 School of Aeronautics and Astronautics, Shanghai Jiao Tong University, No. 800 Dongchuan
Road, Shanghai, 200240, China

2 Department of Engineering Science, University of Oxford, Parks Road, Oxford, OX3 0PL, UK

A. Derivation of equations (2.1) to (2.4)

According to figure 1c, the outer dimensions of the generalized Miura unit cell can be expressed as

$$w = b_1 \sin \xi_1 + b_2 \sin \xi_2, \quad (\text{A1})$$

$$s = v + l, \quad (\text{A2})$$

$$h = a \sin \varphi, \quad (\text{A3})$$

where

$$v = \max\{b_1 \cos \xi_1, b_1 \cos \xi_1 + b_2 \cos \xi_2\}. \quad (\text{A4})$$

$$l = \frac{a \cos \gamma_1}{\cos \xi_1}, \quad (\text{A5})$$

Denote the dihedral angles between facet $V_{11}V_{12}V_{21}V_{22}$ and the x - y plane and between facet $V_{11}V_{12}V_{21}V_{22}$ and the y - z plane by θ_1 and ψ_1 , respectively and the dihedral angles between facet $V_{12}V_{13}V_{22}V_{23}$ and the x - y plane and between facet $V_{12}V_{13}V_{22}V_{23}$ and the y - z plane by θ_2 and ψ_2 , respectively. The following geometric relationships can be found.

$$\tan \xi_1 = \cos \theta_1 \tan \gamma_1, \quad (\text{A6})$$

$$\sin \varphi = \sin \gamma_1 \sin \theta_1, \quad (\text{A7})$$

$$\frac{\cos \xi_1}{\cos \gamma_1} = \frac{\cos \xi_2}{\cos \gamma_2}, \quad (\text{A8})$$

* Corresponding author, E-mail: xiangzhou@sjtu.edu.cn, phone: +86-21-34207538, address: School of Aeronautics and Astronautics, No. 800 Dongchuan Road, Shanghai, 200240, China.

$$\sin \theta_1 \sin \gamma_1 = \sin \theta_2 \sin \gamma_2, \quad (\text{A9})$$

$$\sin \psi_i = \frac{\sin \xi_i}{\sin \gamma_i}, i = 1, 2. \quad (\text{A10})$$

Substituting equations (A5) to (A9) into equations (A1) to (A4) to eliminate φ and ξ_2 , we obtain equations (2.1) to (2.4).

B. Derivations of stretching and bulk moduli

Refer to figure 1c. α_1 , α_2 and β_1 in the expression for U are the dihedral angles between facets $V_{11}V_{12}V_{21}V_{22}$ and $V_{21}V_{22}V_{31}V_{32}$, facets $V_{12}V_{13}V_{22}V_{23}$ and $V_{22}V_{23}V_{32}V_{33}$ and facets $V_{11}V_{12}V_{21}V_{22}$ and $V_{12}V_{13}V_{22}V_{23}$, respectively. They can be expressed as

$$\alpha_i = \pi - 2\theta_i, i = 1, 2, \quad (\text{B1})$$

$$\beta_1 = \psi_1 + (\pi - \psi_2), \quad (\text{B2})$$

where θ_i and ψ_i can be determined from equation (A6) to (A10) as

$$\theta_i = \sin^{-1} \left(\frac{\sin \gamma_1}{\sin \gamma_i} \sqrt{1 - \frac{\tan^2 \xi_1}{\tan^2 \gamma_1}} \right), i = 1, 2, \quad (\text{B3})$$

$$\psi_i = \cos^{-1} \left(\frac{\cos \gamma_i \sqrt{\cos^2 \xi_1 - \cos^2 \gamma_1}}{\cos \gamma_1 \sin \gamma_i} \right), i = 1, 2, \quad (\text{B4})$$

For a general Miura-derivative metamaterial, equations (B1) and (B2) become

$$\alpha_i^j = \pi - 2\theta_i^j, i = 1, \dots, N, j = 1, 2, \quad (\text{B5})$$

$$\beta_i^j = \psi_i^j + (\pi - \psi_{i+1}^j), i = 1, \dots, N, j = 1, 2, \quad (\text{B6})$$

The stretching moduli k_w , k_s and k_h are given by

$$k_w = \frac{d\sigma_w}{dW/W} = \frac{W}{SH(dW/d\xi_1)^2} \left(\frac{d^2U}{d\xi_1^2} - \frac{dU}{d\xi_1} \left(\frac{d^2W/d\xi_1^2}{dW/d\xi_1} + \frac{dS/d\xi_1}{S} + \frac{dH/d\xi_1}{H} \right) \right), \quad (\text{B7})$$

$$k_s = \frac{d\sigma_s}{dS/S} = \frac{S}{HW(dS/d\xi_1)^2} \left(\frac{d^2U}{d\xi_1^2} - \frac{dU}{d\xi_1} \left(\frac{d^2S/d\xi_1^2}{dS/d\xi_1} + \frac{dH/d\xi_1}{H} + \frac{dW/d\xi_1}{W} \right) \right), \quad (\text{B8})$$

$$k_h = \frac{d\sigma_h}{dH/H} = \frac{H}{WS(dH/d\xi_1)^2} \left(\frac{d^2U}{d\xi_1^2} - \frac{dU}{d\xi_1} \left(\frac{d^2H/d\xi_1^2}{dH/d\xi_1} + \frac{dW/d\xi_1}{W} + \frac{dS/d\xi_1}{S} \right) \right), \quad (\text{B9})$$

where

$$\frac{dU}{d\xi_1} = n_3 \sum_{j=1}^2 \left(n_2 \sum_{i=1}^{n_1 N-1} 2k_1 a^j (\beta_i^j - \beta_{i0}^j) \frac{d\beta_i^j}{d\xi_1} + (2n_2 - 1) \sum_{i=1}^{n_1 N} k_2 b_i^j (\alpha_i^j - \alpha_{i0}^j) \frac{d\alpha_i^j}{d\xi_1} \right), \quad (\text{B10})$$

$$\begin{aligned} \frac{d^2 U}{d\xi_1^2} = n_3 \sum_{j=1}^2 \left(n_2 \sum_{i=1}^{n_1 N-1} 2k_1 a^j \left(\left(\frac{d\beta_i^j}{d\xi_1} \right)^2 + (\beta_i^j - \beta_{i0}^j) \frac{d^2 \beta_i^j}{d\xi_1^2} \right) \right. \\ \left. + (2n_2 - 1) \sum_{i=1}^{n_1 N} k_2 b_i^j \left(\left(\frac{d\alpha_i^j}{d\xi_1} \right)^2 + (\alpha_i^j - \alpha_{i0}^j) \frac{d^2 \alpha_i^j}{d\xi_1^2} \right) \right), \end{aligned} \quad (B11)$$

$$\frac{dW}{d\xi_1} = n_1 \sum_{i=1}^N \frac{b_i^1 \cos^2 \gamma_i^1 \sec \gamma_1^1 \cos \xi_1 \sin \xi_1}{\sqrt{\cos^2 \gamma_1^1 - \cos^2 \gamma_i^1 \cos^2 \xi_1}}, \quad (B12)$$

$$\frac{d^2 W}{d\xi_1^2} = n_1 \sum_{i=1}^N \frac{b_i^1 \cos^2 \gamma_i^1 \cos \gamma_1^1 (\cos 2\xi_1 - \cos^2 \gamma_i^1 \sec^2 \gamma_1^1 \cos^4 \xi_1)}{\left(\sqrt{\cos^2 \gamma_1^1 - \cos^2 \gamma_i^1 \cos^2 \xi_1} \right)^3}, \quad (B13)$$

$$\frac{dS}{d\xi_1} = \frac{2n_2 a^1 \cos \gamma_1^1 \sin \xi_1}{\cos^2 \xi_1} - \sum_{i=1}^m \frac{b_i^1 \cos \gamma_i^1 \sin \xi_1}{\cos \gamma_1^1}, \quad (B14)$$

$$\frac{d^2 S}{d\xi_1^2} = \frac{2n_2 a^1 \cos \gamma_1^1 (1 + 2 \tan^2 \xi_1)}{\cos \xi_1} - \sum_{i=1}^m \frac{b_i^1 \cos \gamma_i^1 \cos \xi_1}{\cos \gamma_1^1}, \quad (B15)$$

$$\frac{dH_{M-V}}{d\xi_1} = -n_3 \sum_{j=1}^2 a^j \frac{\cos \gamma_1^j \sec^2 \xi_1 \tan \xi_1}{\sqrt{\tan^2 \gamma_1^j - \tan^2 \xi_1}}, \quad (B16)$$

$$\frac{dH_{V-V}}{d\xi_1} = -n_3 a^2 \frac{\cos \gamma_1^2 \sec^2 \xi_1 \tan \xi_1}{\sqrt{\tan^2 \gamma_1^2 - \tan^2 \xi_1}} - (1 - n_3) a^1 \frac{\cos \gamma_1^1 \sec^2 \xi_1 \tan \xi_1}{\sqrt{\tan^2 \gamma_1^1 - \tan^2 \xi_1}}, \quad (B17)$$

$$\frac{d^2 H_{M-V}}{d\xi_1^2} = -n_3 \sum_{j=1}^2 a^j \frac{\sin \gamma_1^j \tan \gamma_1^j (\sec^2 \xi_1 + 2 \tan^2 \xi_1) - 2 \cos \gamma_1^j \tan^4 \xi_1}{\cos^2 \xi_1 \left(\sqrt{\tan^2 \gamma_1^j - \tan^2 \xi_1} \right)^3}, \quad (B18)$$

$$\begin{aligned} \frac{d^2 H_{V-V}}{d\xi_1^2} = -n_3 a^2 \frac{\sin \gamma_1^2 \tan \gamma_1^2 (\sec^2 \xi_1 + 2 \tan^2 \xi_1) - 2 \cos \gamma_1^2 \tan^4 \xi_1}{\cos^2 \xi_1 \left(\sqrt{\tan^2 \gamma_1^2 - \tan^2 \xi_1} \right)^3} \\ - (1 - n_3) a^1 \frac{\sin \gamma_1^1 \tan \gamma_1^1 (\sec^2 \xi_1 + 2 \tan^2 \xi_1) - 2 \cos \gamma_1^1 \tan^4 \xi_1}{\cos^2 \xi_1 \left(\sqrt{\tan^2 \gamma_1^1 - \tan^2 \xi_1} \right)^3}, \end{aligned} \quad (B19)$$

where in equations (B10) and (B11)

$$\frac{d\alpha_i^j}{d\xi_1} = \frac{2 \cos^2 \gamma_1^j \tan \xi_1}{\cos^2 \xi_1 \sqrt{\sin^2 \gamma_i^j - \sin^2 \gamma_1^j + \cos^2 \gamma_1^j \tan^2 \xi_1} \sqrt{\sin^2 \gamma_1^j - \cos^2 \gamma_1^j \tan^2 \xi_1}}, \quad (B20)$$

$$\begin{aligned} \frac{d^2 \alpha_i^j}{d\xi_1^2} = & \frac{2 \cos^2 \gamma_1^j \sec^2 \xi_1}{\left(\sqrt{\sin^2 \gamma_i^j - \sin^2 \gamma_1^j + \cos^2 \gamma_1^j \tan^2 \xi_1} \sqrt{\sin^2 \gamma_1^j - \cos^2 \gamma_1^j \tan^2 \xi_1} \right)^3} \left(2 \tan^2 \xi_1 (\sin^2 \gamma_1^j \right. \\ & - \cos^2 \gamma_1^j \tan^2 \xi_1) (\sin^2 \gamma_i^j - \sin^2 \gamma_1^j + \cos^2 \gamma_1^j \tan^2 \xi_1) \\ & \left. + \sec^2 \xi_1 (\sin^2 \gamma_i^j \sin^2 \gamma_1^j - \sin^4 \gamma_1^j + \cos^4 \gamma_1^j \tan^4 \xi_1) \right), \end{aligned} \quad (\text{B21})$$

$$\frac{d\beta_i^j}{d\xi_1} = \frac{d\psi_i^j}{d\xi_1} - \frac{d\psi_{i+1}^j}{d\xi_1}, \quad (\text{B22})$$

$$\frac{d^2 \beta_i^j}{d\xi_1^2} = \frac{d^2 \psi_i^j}{d\xi_1^2} - \frac{d^2 \psi_{i+1}^j}{d\xi_1^2}, \quad (\text{B23})$$

where in equations (B22) and (B23)

$$\frac{d\psi_i^j}{d\xi_1} = \frac{\sin \xi_1 \cos \xi_1 \cos \gamma_i^j}{\sqrt{\cos^2 \xi_1 - \cos^2 \gamma_1^j} \sqrt{\cos^2 \gamma_1^j - \cos^2 \gamma_i^j \cos^2 \xi_1}}, \quad (\text{B24})$$

$$\frac{d^2 \psi_i^j}{d\xi_1^2} = \frac{\cos \gamma_i^j \left((\cos^2 \gamma_1^j - \cos^2 \gamma_i^j \sin^2 \gamma_1^j) \cos^4 \xi_1 - \cos^4 \gamma_1^j \cos 2\xi_1 \right)}{\left(\sqrt{\cos^2 \gamma_1^j - \cos^2 \gamma_i^j \cos^2 \xi_1} \sqrt{\cos^2 \xi_1 - \cos^2 \gamma_1^j} \right)^3}. \quad (\text{B25})$$

Finally, the bulk modulus K_V are given by

$$K_V = -\frac{dp}{dV/V} = V \left(\frac{d^2 U / d\xi_1^2}{(dV/d\xi_1)^2} - \frac{dU}{d\xi_1} \frac{d^2 V / d\xi_1^2}{(dV/d\xi_1)^3} \right), \quad (\text{B26})$$

where

$$\frac{dV}{d\xi_1} = SH \frac{dW}{d\xi_1} + WH \frac{dS}{d\xi_1} + WS \frac{dH}{d\xi_1}, \quad (\text{B27})$$

$$\frac{d^2 V}{d\xi_1^2} = 2W \frac{dS}{d\xi_1} \frac{dH}{d\xi_1} + 2S \frac{dW}{d\xi_1} \frac{dH}{d\xi_1} + 2H \frac{dW}{d\xi_1} \frac{dS}{d\xi_1} + SH \frac{d^2 W}{d\xi_1^2} + WH \frac{d^2 S}{d\xi_1^2} + WS \frac{d^2 H}{d\xi_1^2}. \quad (\text{B28})$$